A Numerical Theory for Impedance Eduction in Three-Dimensional Normal Incidence Tubes

Willie R. Watson* and Michael G. Jones†
NASA Langley Research Center, Hampton, Virginia 23681-2199

A method for educing the locally-reacting acoustic impedance of a test sample mounted in a 3-D normal incidence impedance tube is presented and validated. The unique feature of the method is that the excitation frequency (or duct geometry) may be such that high-order duct modes may exist. The method educes the impedance, iteratively, by minimizing an objective function consisting of the difference between the measured and numerically computed acoustic pressure at preselected measurement points in the duct. The method is validated on planar and high-order mode sources with data synthesized from exact mode theory. These data are then subjected to random jitter to simulate the effects of measurement uncertainties on the educed impedance spectrum. The primary conclusions of the study are 1) Without random jitter the method is in excellent agreement with that for known impedance samples, and 2) Random jitter that is compatible to that found in a typical experiment has minimal impact on the accuracy of the educed impedance.

I. Introduction

Efficient duct treatments for broadband noise suppression in turbofan engine ducts remain critical to the development of environmentally acceptable commercial aircraft. To this end, an accurate knowledge of duct-treatment impedance in real flows is critical to effective liner design. In the absence of grazing flow, the normal incidence impedance tube (NIT) is used almost universally for obtaining the acoustic impedance of test liner specimens. Current NIT tests use the standard two-microphone method[1] to determine the impedance of uniform samples at frequencies for which only the plane wave mode propagates along the duct.

Recently, the NASA Langley Research Center added a dual waveguide normal incidence tube (DWNIT) to its liner technology facility. The DWNIT can be configured as a conventional normal incidence tube, in which the sound field is introduced at one end of the duct and the test sample is placed at the opposite end, mounted perpendicular to the incoming sound field. A lengthwise partition can also be installed in the DWNIT so that the duct is subdivided into two separate waveguides. In the first configuration, two electromagnetic acoustic drivers combine to provide the desired sound source. In the second configuration, a single driver is used to supply the sound field in each of the waveguides. This latter option allows the user to simulate complex acoustic environments at the surface of the sample. The DWNIT is also equipped with acoustic probes that are located at three axial positions away from the sample surface. Data acquired with these probes will allow determination of the high-order modal content of the acoustic field. Thus, the upper-frequency capability of the DWNIT is limited by the capability of the acoustic drivers to generate a sufficient amount of sound and the ability to accommodate the effects of high-order duct modes (that cut-on at the higher frequencies) in the impedance eduction. The current research effort is intended to provide support to the DWNIT for impedance eduction when high-order modes are present. The paper has three primary objectives: 1) to develop a method to educe the impedance of a test sample when high-order modes are cut-on, 2) to validate the method using data synthesized from mode theory, and 3) to test the integrity of the method in the presence of uncertainties by applying random jitter to the sound pressure level and phase data. A testing of the proposed method with measured DWNIT data is beyond the scope of this paper but will be the subject of a second investigation.

The current paper is organized into six Sections. Section II describes the physical problem along with the measurements that are required. Section III presents a description of the governing differential equations and boundary conditions as well as the impedance eduction methodology. The eduction method requires data in the form of duct modes. Therefore, Section IV presents a least square method that computes the energy in these duct modes from the complex acoustic pressure at preselected points in the duct. Results are presented in Section V, and the primary conclusions of the paper are presented in Section VI.

*Senior Research Scientist, Research Directorate, Computational AeroSciences Branch, Liner Physics Group, Associate Fellow AIAA.
†Senior Research Scientist, Research Directorate, Structural Acoustics Branch, Liner Physics Group, Associate Fellow AIAA.

II. Description of Physical Problem

Figure 1 shows a schematic of the Langley DWNIT and the right-handed coordinate system used in this study. The axial, vertical, and horizontal coordinates are denoted by z, x, and y, respectively. The duct is assumed to have uniform

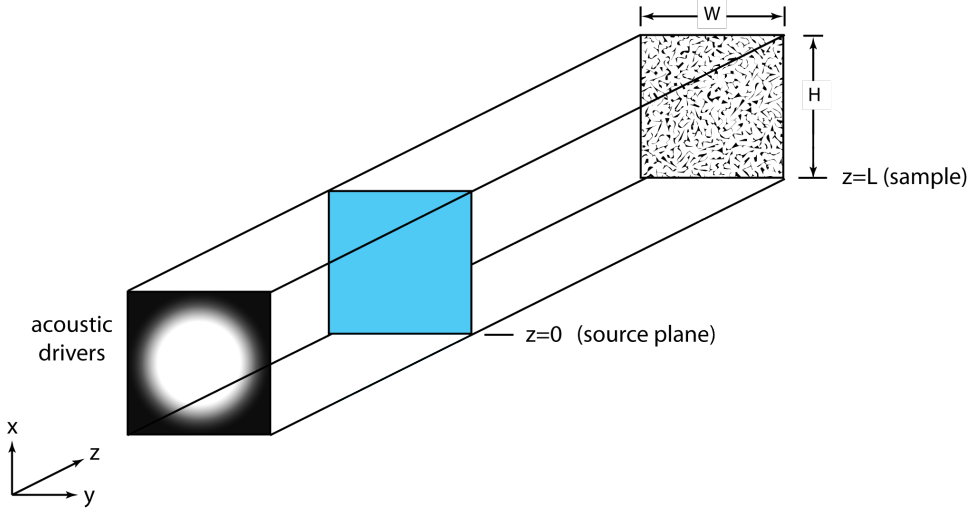

Figure 1. Schematic of the LaRC Dual Waveguide Normal incidence Tube (DWNIT).

height, H, and width, W, and the left, right, upper, and lower walls of the duct are rigid. Sound is generated by acoustic drivers that are located upstream of the test sample and the source plane is located at $z = 0$ as shown. For the sake of convenience, the origin of the coordinate system is located in the lower left corner of the source plane. The acoustic material is mounted in the sample end at $z = L$, and is assumed to be locally reacting. The normalized impedance of this acoustic material is denoted by ζ, and this impedance is normalized with the characteristic impedance, $\rho_0 c_0$, of the air in the duct. Here ρ_0 and c_0 are the ambient density and speed of sound, respectively, in the duct. Transients in the duct are assumed to have been dissipated by viscous forces so that the acoustic field is assumed to be at a periodic steady-state with a harmonic time dependence of the form $e^{i\omega t}$. Here, $i = \sqrt{-1}$, is the unit imaginary number, $\omega = 2\pi f$ is the angular frequency, f is the excitation frequency, and t denotes time in seconds. Further, the excitation frequency and duct geometry are such that higher-order duct modes may be cut-on in one or both cross-sectional directions simultaneously. The problem at hand is: given the acoustic source pressure and the measured acoustic pressure profiles at two axial stations between the source and sample end of the duct, determine the unknown normalized acoustic impedance ζ, of the test sample.

III. The Impedance Eduction Methodology

The impedance eduction method proposed here is an indirect method because it educes the impedance using an iterative method. This method is similar to that presented by Watson[2] for grazing incidence sound in two space dimensions. However, in this paper, the method is extended to three space dimensions. In addition, the sound impinges on the liner at normal incidence instead of at grazing incidence as in the NASA Langley Grazing Flow Impedance Tube Facility.[2]

To begin, the equation that describes the propagation of linearized steady-state acoustic pressure disturbances within the duct depicted in Fig. 1 is the three dimensional Helmholtz equation[3]

$$\nabla^2 p + k^2 p = 0 \tag{1}$$

where ∇^2 is the 3D Laplace operator, $k = \omega/c_0$ is the free space wavenumber, and p is the acoustic pressure field in the duct. The upper, lower, and sidewalls of the duct are rigid so that the boundary conditions along these walls are

$$\vec{\nabla} p \bullet \vec{n} = 0 \tag{2}$$

Here $\vec{\nabla}$ is the gradient vector and $\vec{n}$ is the outward pointing unit normal to the duct wall. The acoustic material

mounted into the sample end is locally-reacting so that the boundary condition at the sample end is[4]

$$\vec{\nabla} p \bullet \vec{n} = -ik\frac{p}{\zeta} \tag{3}$$

Across the source plane of the duct ($z = 0$) the acoustic source pressure profile, $G_0(x,y)$, is known

$$p(0,x,y) = G_0(x,y) \tag{4}$$

Note that in the DWNIT the source pressure, $G_0(x,y)$ will be measured. Finally at two axial planes between the source and sample end of the tube ($z = L_1$ and $z = L_2$), the acoustic pressure profiles are also known (i.e., measured in the DWNIT)

$$p(L_1,x,y) = G_1(x,y), \quad p(L_2,x,y) = G_2(x,y) \tag{5}$$

The dependence of G_0, G_1 and G_2 on the transverse and horizontal coordinates, (x,y), implies that either the source frequency or the cross-sectional area of the duct are sufficiently large that high-order modes are cut-on.

Given the source plane acoustic pressure profile, $G_0(x,y)$, and impedance function, ζ, Eqs. (1)−(4) constitute a well-posed boundary value problem (BVP) that can be solved uniquely to obtain the acoustic pressure field everywhere in the duct. This uniqueness proof can be found in any elementary text on partial differential equations.[3] Conversely, because the acoustic pressure field (with the test sample installed) is also known at the axial stations, $z = L_1$ and $z = L_2$, the unknown impedance, ζ, can be determined using an iterative procedure.

The analysis begins by solving the BVP defined in Eqs. (1)−(4) numerically using a 3-D finite element method (FEM). The details of the 3-D FEM solution are rather lengthy and are presented in the appendix of this paper for the interested reader. A numerical procedure is then developed to educe the unknown impedance, ζ, of the test sample by using both this FEM and the known solutions at the axial stations, $z = L_1$ and $z = L_2$. Thus, if the impedance of the test sample is properly chosen, then the acoustic pressure profiles computed from the FEM will match the measured profiles to within some tolerance. We therefore form an objective function, $\psi(\zeta)$, defined as

$$\psi(\zeta) = \frac{1}{(NX)(NY)} \sum_{r=1}^{NX} \sum_{s=1}^{NY} \| G_1(x_r,y_s) - p_{\mathrm{FEM}}(L_1,x_r,y_s) \| + \| G_2(x_r,y_s) - p_{\mathrm{FEM}}(L_2,x_r,y_s) \| \tag{6}$$

where NX, NY are the number of axial grid lines in the x and y directions, respectively, and the subscript FEM denotes the pressure profiles obtained from the finite element solution. Here, x_r, y_s are the intersections of the x and y gridlines in the FEM grid (see the appendix).

Now the value of ζ that minimizes the objective function, $\psi(\zeta)$, is the normalized impedance function of the test sample. An automated search procedure is therefore implemented with the use of an optimization algorithm. The optimization algorithm is a modification of the Davidon-Fletcher-Powell (DFP) optimization algorithm. The DFP optimization algorithm was first proposed by Davidon[5] and was later reformulated and popularized by Fletcher and Powell.[6] In the procedure used here, an analytical expression for the gradient of $\psi(\zeta)$ is not available. Therefore, the gradient of $\psi(\zeta)$ is computed numerically by using a finite difference approximation that was developed by Stewart.[7]

IV. Acquiring the Eduction Data

The acoustic pressure data ($G_1(x,y)$ and $G_2(x,y)$) that are required to perform the impedance eduction are obtained using mode synthesis. To begin, the acoustic pressure field in the duct is expanded as a series of hard wall duct modes:

$$p(z,x,y) = A^+_{nm}\left(e^{-iK_{nm}z} + R_{nm}e^{iK_{nm}z}\right)P_{nm}(x,y), \quad R_{nm} = \frac{\left(\frac{K_{nm}}{k} - \frac{1}{\zeta}\right)}{\left(\frac{K_{nm}}{k} + \frac{1}{\zeta}\right)} e^{-2iK_{nm}L} \tag{7}$$

where the hard wall duct modes, $P_{nm}(x,y)$, are

$$P_{nm}(x,y) = \cos\left(\frac{n\pi x}{H}\right)\cos\left(\frac{m\pi y}{W}\right) \tag{8}$$

and the axial propagation constants, K_{nm}, are

$$K_{nm} = k\sqrt{1 - \left[(n\pi/kH)^2 + (m\pi/kW)^2\right]} \tag{9}$$

Here, A^{+}_{nm} are the complex mode coefficients for the right-running modes. These complex mode coefficients are determined by expanding each of the functions $G_0(x,y)$, $G_1(x,y)$ and $G_2(x,y)$ as a series of hard wall duct modes as described in the subsequent paragraphs. Further, each K_{nm} determines whether the mode is cut-on or cut-off. Right-running modes that are cut-off decay as they propagate along the positive z axis (i.e., $\Im(K_{nm}) < 0$), whereas left running cut-off modes decay as they propagate along the negative z axis (i.e., $\Im(K_{nm}) > 0$). Further, if K_{nm} is wholly real ($\Im(K_{nm}) = 0$), the acoustic mode propagates without decay and is said to be cut-on. In this situation, the axial propagation constant of the right-running modes will have a positive real part (i.e., $\Re(K_{nm}) > 0$) and those of the left-running modes will have a negative real part (i.e., $\Re(K_{nm}) < 0$), respectively.

Now the primary goal of the multi-modal analysis method is to provide a means to measure the right-running and left-running mode coefficients, $A^{\pm}_{nm}$, that are needed in Eq. (7). To measure the mode coefficients, three measurement planes are located in the DWNIT. Figure 2 shows the axial location of these three measurement planes. The first axial

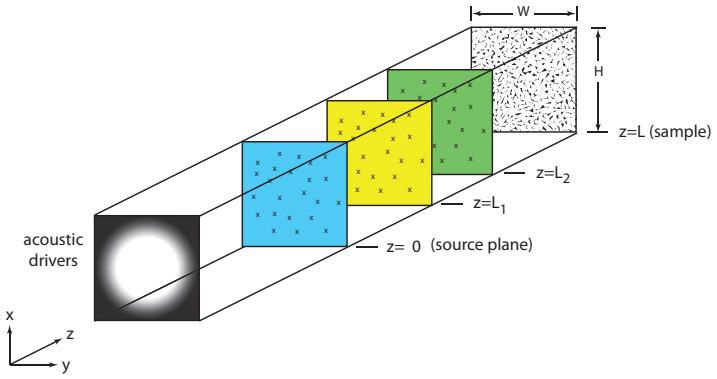

Figure 2. Axial location of measurement planes in the DWNIT.

measurement plane is the source plane and is located at $z = 0$. The second and third measurement planes are located downstream of the source plane at $z = L_1$ and $z = L_2$, respectively. In each measurement plane, the time-harmonic acoustic pressure is assumed to be measured at Q locations, $(x_1,y_1),(x_2,y_2),\ldots(x_Q,y_Q)$ with acoustic probes.

Evaluating Eq. (7) at the Q points across the source plane gives a total of Q equations in $2NM$ unknowns of the form

$$\sum_{n=0}^{N-1}\sum_{m=0}^{M-1}\left(A^{+}_{nm}+A^{-}_{nm}\right)P_{nm}(x_q,y_q) = G_0(x_q,y_q), \quad q = 1,2,\ldots Q \tag{10}$$

where N,M are the total number of vertical and horizontal modes, respectively, in the mode expansion. Values of N and M are assumed sufficiently large that all cut-on modes are included in the mode series. Evaluating Eq. (7) at $z = L_1$ and $z = L_2$ gives two additional equations of the form

$$\sum_{n=0}^{N-1}\sum_{m=0}^{M-1}\left(A^{+}_{nm}e^{-iK_{nm}L_1}+A^{-}_{nm}e^{iK_{nm}L_1}\right)P_{nm}(x_q,y_q) = G_1(x_q,y_q), \quad q = 1,2,\ldots Q \tag{11}$$

$$\sum_{n=0}^{N-1}\sum_{m=0}^{M-1}\left(A^{+}_{nm}e^{-iK_{nm}L_2}+A^{-}_{nm}e^{iK_{nm}L_2}\right)P_{nm}(x_q,y_q) = G_2(x_q,y_q), \quad q = 1,2,\ldots Q \tag{12}$$

Equations (10)−(12) are now combined into a system of 3Q linear equations in 2NM unknowns of the form

$$[C]\{A^{\pm}\} = \{p\} \tag{13}$$

where $\{A^{\pm}\}$ is a column vector of length $2NM$ that contains the $2NM$ right running and left-running mode coefficients, $\{p\}$ is a vector of length $3Q$ containing the measured acoustic pressures at the axial locations $z = 0$, $z = L_1$, and $z = L_2$, respectively, and [C] is a $3Q \times 2NM$ complex matrix. Equation (13) is solved using the method of least squares to obtain the mode coefficients. These mode coefficients are then substituted into the mode series defined by Eq. (7) to determine the acoustic pressure field at $z = L_1$ and $z = L_2$.

V. Results and Discussion

An in-house computer code that implements the impedance eduction methodology has been developed. In the current implementation, the resistance, θ, and reactance, χ, of the test sample are the design variables ($\zeta = \theta + i\chi$). Results are restricted to the geometry of the Langley DWNIT. The DWNIT has a 51 $\times$ 51 mm cross-section and the computational domain is 102 mm in length (i.e., $L = 102$ mm). The data required to perform impedance eduction (referred to here as the eduction data) are assumed to be obtained at standard atmospheric conditions so that c_0=343 m/s. The two measurement probes are located at $z = L_1 = 203$ mm and $z = L_2 = 406$ mm.

Results are presented using simulated data and then the simulated data is subjected to random jitter of $\pm$ 2 dB in the sound pressure level and $\pm$ 2 degrees in the phase. This amount of random jitter is larger than that expected from typical measurements in the DWNIT. The distribution is assumed Gaussian. The random jitter is used to determine the effects of uncertainties on the robustness of the impedance eduction method. For this study there are 20 measurement points in each plane (i.e., $Q = 20$) distributed in an arbitrary manner across the "measurement plane." Table 1 shows the (x,y) locations in millimeters for each of the twenty measure points, q. Thus, the system matrix, $[C]$ (see Eq. (13))

Table 1. (x,y) locations for 20 measurement points

q	x(mm)	y(mm)	q	x (mm)	y (mm)	q	x(mm)	y(mm)	q	x(mm)	y(mm)
1	33.78	14.99	6	46.23	9.14	11	42.93	32.26	16	46.23	14.73
2	6.35	9.65	7	30.23	45.72	12	5.08	27.69	17	30.48	14.48
3	11.68	18.29	8	33.27	30.48	13	9.65	26.92	18	45.47	24.64
4	33.78	7.37	9	45.97	38.61	14	30.73	32.51	19	15.74	15.24
5	04.83	39.88	10	9.40	44.96	15	16.51	17.27	20	33.78	41.91

has a total of sixty rows. For all calculations presented in this section a total of six modes (three right-running and three left-running) are included in the mode expansion at each frequency (i.e., $N+M$=3). Thus the mode expansion is performed with the (0,0), (0,1), and (1,0) right and left-running modes.

To account for random jitter, each complex acoustic pressure profile $(G_1(x_q,y_q), G_2(x_q,y_q))$ are expressed as a sound pressure level and a phase at each measurement point (x_q,y_q)

$$G_1(x_q,y_q) = SPL_1(x_q,y_q)e^{i\phi_1(x_q,y_q)}, \quad G_2(x_q,y_q) = SPL_2(x_q,y_q)e^{i\phi_2(x_q,y_q)} \tag{14}$$

Here, $SPL_1(x_q,y_q)$ and $SPL_1(x_q,y_q)$ are sound pressure levels and $\phi_1(x_q,y_q)$ and $\phi_2(x_q,y_q)$ are the phases. A random number generator is used to randomly change the sound pressure levels by $\pm$2 dB and phase by $\pm$2 degrees at each measurement point (x_q,y_q).

Three examples are now presented to demonstrate the accuracy and robustness of the impedance eduction methodology. The input data for the impedance eductions (i.e., $G_1(x,y)$ and $G_2(x,y)$) are simulated from the exact solution for a known impedance. In the first example problem, the eduction data correspond to those for an anechoic termination. In the second example problem, the eduction data correspond to those when a rigid wall is inserted into the sample end. In the final example problem, the eduction data correspond to those of a sound absorbing material with known impedance. For each example problem, the impedance is first educed using a plane wave source. Afterward, the source is changed to a high-order mode source to demonstrate that the impedance is again accurately educed. Finally, random jitter is applied to the eduction data to simulate the effects of uncertainties on the accuracy of the impedance eduction method.

The impedance eduction method uses an evenly spaced FEM grid with $NX = NY = 21$, and $NZ = 81$ (see the appendix). A grid refinement study revealed no significant changes in educed impedance by further refining the FEM grid. Further, the optimization algorithm was initialized using several values of the resistance, θ, and the reactance, χ, but no noticeable change in the educed impedance was observed. The impedance eductions were run on an SGI computer with sixteen 2.5 GHz Xeon E5-2670 processors and the computer code consumed 12 GBytes of RAM and approximately 30 minutes of wall clock time per frequency. The primary focus of the results to follow is to demonstrate that over the frequency range of interest in the DWNIT (i.e., frequencies up to 10.0 kHz) the impedance eduction procedure is accurate and robust for both planar and high-order mode sources and is minimally affected by random error.

A. Educed Impedance of an Anechoic Termination

When the sound source consists of only a single right-running mode at 120 dB incident sound pressure level ($A^-_{nm} = 0, A^+_{nm} = 20$ Pa), an exact analytical solution for ζ can be written. Here ζ is referred to as the normalized anechoic termination impedance because it allows the chosen source mode to exit at $z = L$ without reflecting. The exact expression for the normalized anechoic termination impedance can be derived using the exact mode solution for the (n,m)th mode

$$\zeta = \frac{k}{K_{nm}} \tag{15}$$

The acoustic pressure profiles at $z = L_1$ and $z = L_2$ that are needed for the impedance eductions are obtained from the exact mode solution

$$p(z,x,y) = A^+_{nm} e^{-iK_{nm}z} P_{nm}(x,y) \tag{16}$$

The details used to obtain the eduction data are as follows:

1. The right running mode coefficient is set to a 120 dB sound pressure level (i.e., $A^+_{nm} = 20$ Pa).
2. The exact solution given by Eq. (16) is used to determine $G_0(x,y)$, $G_1(x,y)$ and $G_2(x,y)$. (See Eqs. (4)−(5) at the 20 preselected measurement points given in Table 1.)
3. Equation (13) is solved to obtain the right and left-running mode coefficients for the (0,0), (1,0), and (0,1) modes.
4. These right and left-running mode coefficients are used to obtain the eduction data (i.e., $G_1(x_r,y_s)$ and $G_2(x_r,y_s)$) at each point (x_r,y_s) of the finite element grid with the mode expansion in Eq. (16).
5. The objective function, $\psi(\zeta)$, is formed and minimized to obtain the anechoic termination impedance, ζ.

Fig. 3 compares the normalized resistance and reactance spectra educed (without random jitter) for an outgoing plane wave ($n = 0$, $m = 0$) with the exact spectra given by Eq. (15). Results are computed in 0.2 kHz increments

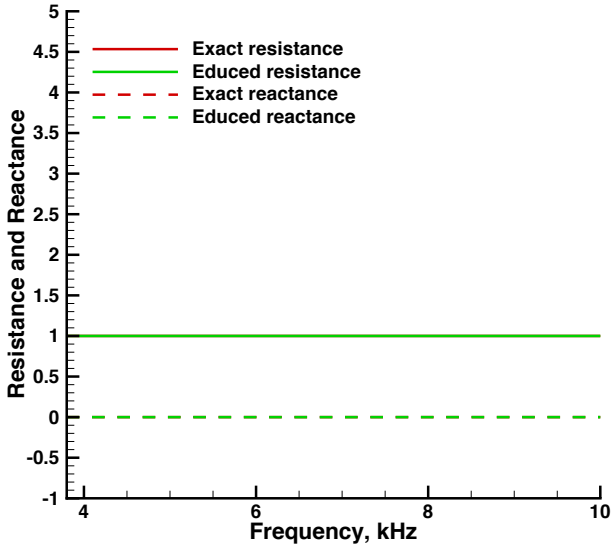

Figure 3. Anechoic termination impedance for the plane wave mode (without random jitter).

starting at 0.36 kHz and terminating at 10.0 kHz. The normalized resistance spectra (solid curves) and reactance spectra (dashed curves) cannot be distinguished from each other. Figure 4 shows results similar to that in Fig. 3 but for a higher-order mode source ($n = 1$, $m = 0$). The cut-on frequency for this source mode is below 3.6 kHz so results are shown only for those frequencies greater than the cut-on frequency (i.e., the cut-off modes do not carry acoustic energy down the duct). Further, the coefficient matrix $[C]$ is poorly conditioned for frequencies below the cut-on frequency so

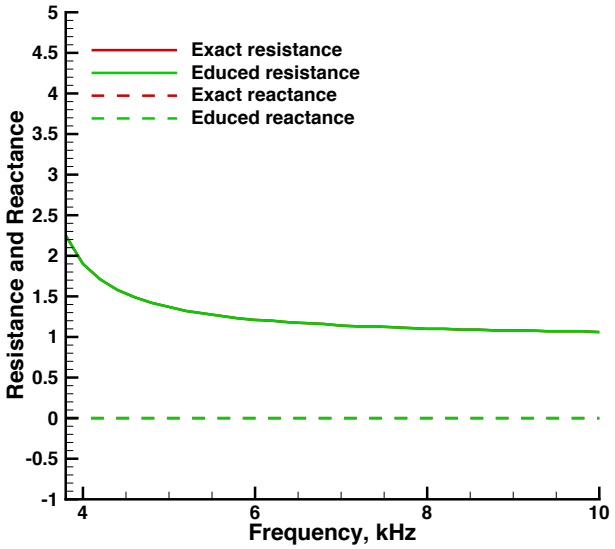

Figure 4. Anechoic termination impedance of higher-order mode source (without random jitter).

that the solution to Eq. (13) may not adequately capture the energy in cut-off modes. Note that although the educed normalized reactance remains zero for this high-order mode, the educed normalized resistance is not unity (as with the plane wave source) but asymptotes to unity at the high frequency end of the spectrum. The educed normalized impedance for this higher-order mode source is in excellent agreement with the exact value.

B. Educed Impedance of a Rigid Wall

We now demonstrate the ability of impedance eduction method to extract the normalize admittance, $\beta = \frac{1}{\zeta}$, for a rigid wall insert. In this situation, it is easily demonstrated that the left-running wave coefficient, A^-_{nm}, is related to the right-running wave coefficient by the relation

$$A^-_{nm} = A^+_{nm} e^{-2K_{nm}L} \tag{17}$$

Here the right-running mode coefficient is set to an incident sound pressure level of 120 dB ($A^+_{nm} = 20$ Pa) and the left-running mode coefficient is computed from Eq. (17). Given $A^\pm_{nm}$, the impedance eduction code is used to educe the admittance, β for the rigid wall.

The normalized conductance ($\Re(\beta)$) and susceptance ($\Im(\beta)$) for the plane wave source were educed with and without random jitter. These results are not shown for the sake of brevity. However, the educed normalized conductance and susceptance were accurate to six decimal digits of precision in the absence of random jitter. When random jitter was added, the admittance educed differed from that without random jitter only in the third decimal digit of precision. Further, the authors have shown that the impact of random jitter on a rigid wall is to affect the precision of the educed admittance in the first decimal digit when the sound is at grazing incidence.[2] Thus, a normal incidence impedance eduction may be more accurate than a grazing incidence impedance eduction under similar conditions of measurement uncertainty. Similar results are observed when a higher-order mode (the $(0,1)$ or the $(1,0)$ modes) are used as the sound source. For example, Fig. 5 shows results when the $n = 1$ and $m = 0$ mode is used as the sound source in the rigid wall duct. Here, the educed normalized admittance is plotted starting with the cut-on frequency of the source mode (i.e., approximately 3.6 kHz) and ending at 10.0 kHz. Results are shown with and without random jitter. Note that the impedance eduction code educes the normalized admittance of the rigid wall with good accuracy without random jitter. The random jitter produces little change in educed admittance except for the spike in susceptance at 7.6 kHz.

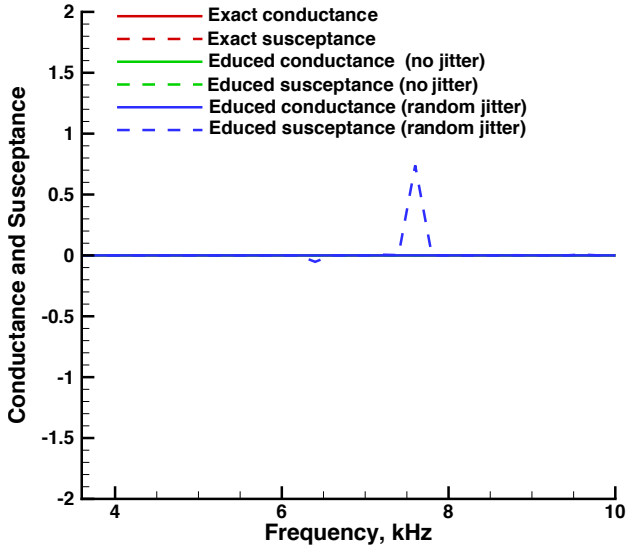

Figure 5. Educed admittance for a rigid wall insert for a high-order mode source.

C. Educed Impedance for a Ceramic Liner

In this third and final example using simulated data, impedances are educed for a ceramic tubular liner (see Fig. 6) whose impedance can be predicted using first principles.[8] When a single mode propagates down the duct, the exact solution is given by Eq. (7).

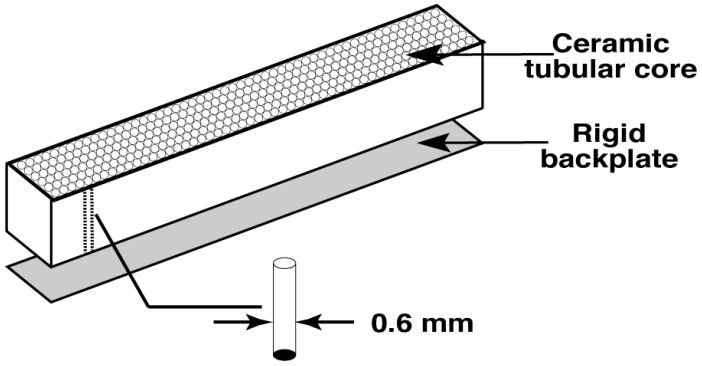

Figure 6. Schematic of ceramic tubular liner.

Figures 7 and 8 show the educed normalized impedance (i.e., the normalized resistance and reactance spectra) for the ceramic tubular liner for a plane wave (the (0,0) mode) and a high-order mode source (the (1,0) mode), respectively. The incident sound pressure level is set at 120 dB ($A_{00}^{+} = 20$ Pa for the plane wave source, $A_{10}^{+} = 20$ Pa for the high-order mode source). Results are plotted commencing with the frequency just beyond the cut-on frequency of the source mode and terminating at 10.0 kHz. Just as with the previous two examples, at this chosen level of precision, the educed normalized impedance spectra for the liner are in excellent agreement with that predicted from a first principle evaluation[8] for both the plane wave and the high-order mode source. Here the resistance and reactance obtained from the first principle result is referred to as the "exact" resistance and reactance. There is no effect of the random jitter on the educed impedance for the planar source (see Fig. (7)). There is an effect of the random jitter for the high-order mode source at 7.6 kHz but the effect is extremely small at all other frequencies (Fig. (8)).

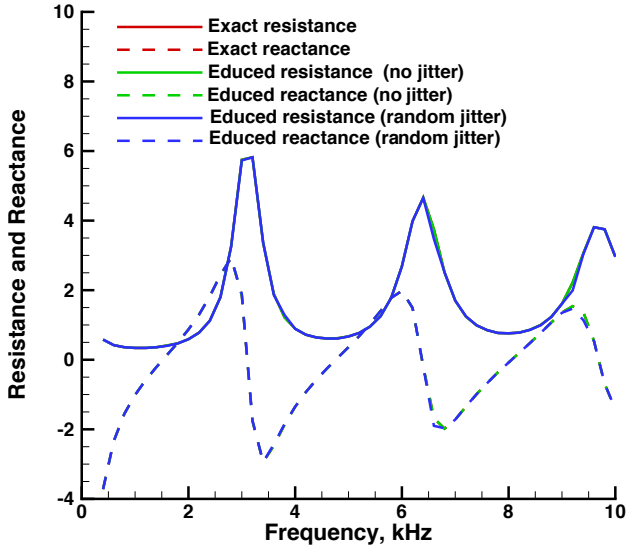

Figure 7. Impedance spectra for ceramic tubular with a plane wave source.

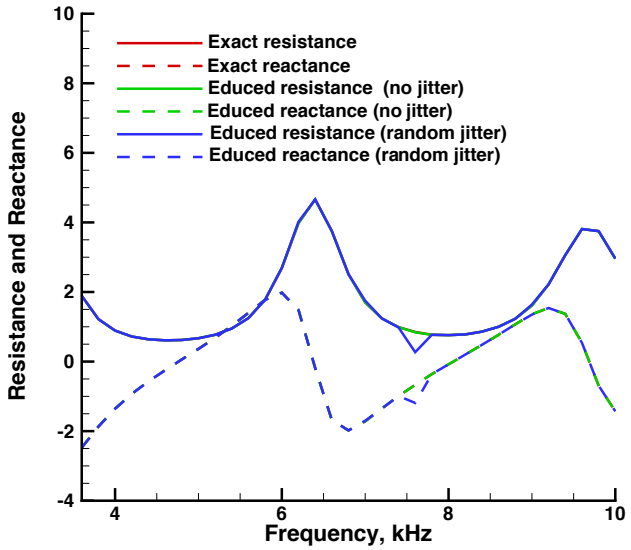

Figure 8. Impedance spectra for ceramic tubular with a high-order mode source.

VI. Conclusions

This paper has presented a method for educing the impedance of a liner that is installed in a normal incidence impedance tube. The basic assumptions are that either the source frequency or the duct cross-sectional area is sufficiently large that high-order duct modes propagate. Based on the results of this paper the following conclusions are drawn:

1. In the absence of random jitter, the method accurately predicts the known impedance for planar and high-order mode sources for excitation frequencies above the cut-on frequency of source modes.

2. The effects of random jitter of ± 2 dB in the sound pressure level and $\pm$ 2 degree in phase have a minimal impact on the accuracy of the educed impedance.

3. The current normal incidence method is less sensitive to uncertainties in the measurement than the grazing incidence method of an earlier paper. This tends to promote the use of normal incidence impedance tubes to educe impedance in environments for which the uncertainties in the measurements are high.

The results of this study are sufficiently encouraging to warrant additional studies with real test data such as that the DWNIT can provide. This will allow impedance spectra to be educed at larger frequencies where high-order duct modes must be take into account.

References

[1]Chung, J. Y. and Blaser, D. A., " Transfer Function Method of Measuring in-Duct Acoustic Properties: I. Theory," *Journal of the Acoustical Society of America*, Vol. 68, No. 3, Sept. 1980, pp. 907−921.

[2]Watson, W. R., Jones, M. G., and Parrott, T. L., "Validation of an Impedance Eduction Method in Flow," *AIAA Journal*, Vol. 37, No. 7, July 1999, pp. 818−824.

[3]Morse, Philip M. and Ingard, K. Uno, *Theoretical Acoustics*, McGraw-Hill, New York, 1968, pp. 495−496.

[4]Myers, M. K., "On the Acoustic Boundary Condition in the Presence of Flow," *Journal of Sound and Vibration*, Vol. 71, No. 3, 1980, pp. 429−434.

[5]Davidon, W. C., " Variable Metric Methods for Minimization,"Argonne National Labs Report ANL−5990, 1959.

[6]Fletcher, R. and Powell, M. J. D., "A Rapidly Convergent Descent Method for Minimization," *The Computer Journal*, Vol. 6, No. 2, 1963, pp. 163−168.

[7]Stewart, G. W. III, "A Modification of Davidon's Minimization Method to Accept Difference Approximations of Derivatives," *Journal of ACM*, Vol. 14, No. 1, 1967, pp 72−83.

[8]Parrott, T. L. and Jones, M. G., "Parallel-element Liner Impedances for Improved Absorption of Broadband Sound in Ducts," *Noise Control Engineering Journal*, Vol. 43, No. 6, Nov 1995, pp. 183−195.

[9]Chandrakant, S. and Abel, John F., *Introduction to the Finite Element Method*, Van Nostrand Reinhold, New York, 1972, pp. 176−193.

Appendix: The Finite Element Method

This appendix gives more detail concerning the 3D finite element method discussed in the main body of this paper. Figure 9 shows the FEM discretization of the duct depicted in Fig. 1. Within the computational domain ($0 \le z \le L$, $0 \le x \le H$, $0 \le y \le W$) a grid consisting of NZ, NX and NY unevenly spaced grid lines is used in the z, x, and y directions of the duct, respectively. Note that the FEM discretization divides the computational domain into $(NZ-1)(NX-1)(NY-1)$ brick elements as shown in Fig. 9. A typical brick element with vertical, horizontal, and axial dimensions h, w and l is shown in Fig. 10.

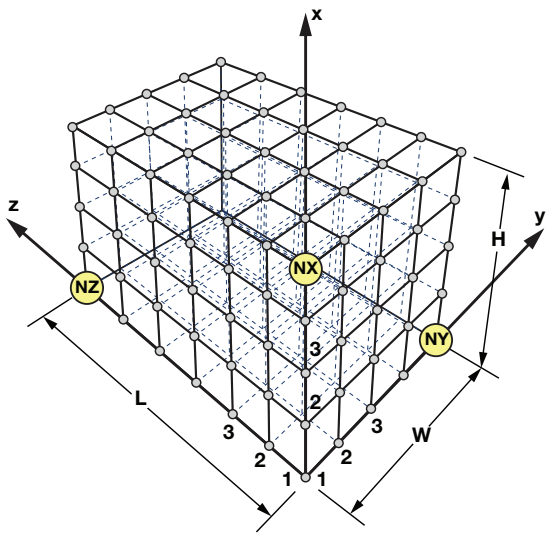

Figure 9. Finite element discretization of the three-dimensional duct.

Each brick element consists of eight local node numbers labeled 1, 2, …, 8, respectively. Within each element,

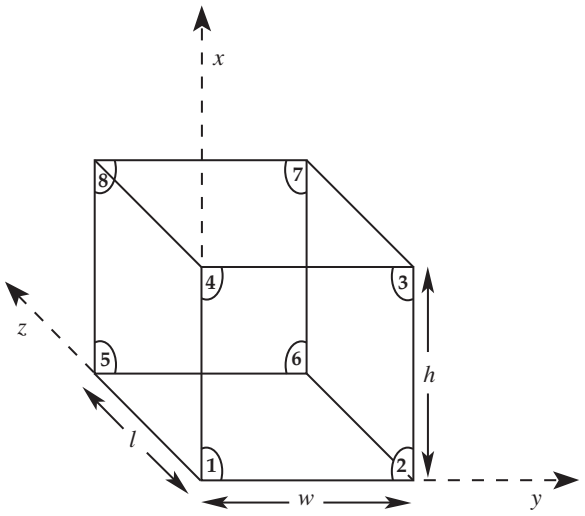

Figure 10. A typical brick element.

$p(z,x,y)$ is approximated as a combination of 64 linearly independent basis functions, $F_I(z,x,y)$

$$p = \sum_{I=1}^{I=64} F_I(z,x,y)\Phi_I \tag{18}$$

The basis functions, $F_I(z,x,y)$, can be found in standard finite element texts[9] and are not listed explicitly in this appendix. However, each of the 64 basis functions, F_I, and nodal degrees of freedom Φ_I are constructed such that the acoustic pressure, $p(z,x,y)$ and its normal derivative, $\nabla p \bullet \vec{n}$, are continuous across inter-element boundaries. For example, $F_1(z,x,y) = \mathcal{F}_1(z,l)\mathcal{F}_1(x,h)\mathcal{F}_1(y,w)$, $F_2(z,x,y) = \mathcal{F}_2(z,l)\mathcal{F}_1(x,h)\mathcal{F}_1(y,w)$, … where the 1D cubic Hermite polynomials are

$$\mathcal{F}_1(z,l) = 1 - 3z^2/l^2 + 2z^3/l^3, \quad \mathcal{F}_2(z,l) = z(z/l-1)^2, \tag{19}$$

$$\mathcal{F}_3(z,l) = (z^2/l^2)(3-2z/l), \quad \mathcal{F}_4(z,l) = (z^2/l)(z/l-1) \tag{20}$$

Further, Φ_I ($I = 1,2,\ldots 64$) contains the values of the acoustic pressure, p, and its derivatives $\frac{\partial p}{\partial z}$, $\frac{\partial p}{\partial x}$, $\frac{\partial p}{\partial y}$, $\frac{\partial^2 p}{\partial x \partial y}$, $\frac{\partial^2 p}{\partial x \partial z}$, $\frac{\partial^2 p}{\partial y \partial z}$, $\frac{\partial^3 p}{\partial x \partial y \partial z}$ at the eight local nodes of the brick element.

Galerkin's finite element method is used to minimize the field error and develop the element stiffness matrix. The field error function is defined as

$$E = \nabla^2 p + k^2 p \tag{21}$$

Contributions to the minimization of the error over all the finite elements are

$$\sum_{\text{elements}} \int_V E F_I dV = \sum_{\text{elements}} \int_V \left[\nabla^2 p + k^2 p\right] F_I dV \tag{22}$$

where the sum in Eq. (22) is carried out using the usual rules of a finite element assembly. The second derivative terms in Eq (22) are reduced to first derivatives using Green's second identity

$$\sum_{\text{elements}} \int_V E F_I dV = \sum_{\text{elements}} \int_V \left[-\vec{\nabla} p \bullet \vec{\nabla} F_I + k^2 p F_I\right] dV + \sum_{\text{elements}} \int_S \vec{\nabla} p \bullet \vec{n} F_I dS \tag{23}$$

The contributions to the surface integral

$$\sum_{\text{elements}} \int_S \vec{\nabla} p \bullet \vec{n} F_I dS \tag{24}$$

sum to zero for all interior and boundary elements, except those that lie along the sample end of the impedance tube and the source plane. Substituting the boundary condition at the sample end into the surface integral in Eq. (24) allows the boundary condition (Eq. (3)) to be implemented in weak form

$$\sum_{\text{elements}} \int_S \vec{\nabla} p \bullet \vec{n} F_I dS = -\beta \sum_{\text{elements}} ik \int_S p F_I dS \tag{25}$$

The system of equations resulting from the finite element assembly of the $(NZ-1)(NX-1)(NY-1)$ brick elements is of the form

$$[B(\zeta)]\{\Phi\} = \{G_0\} \tag{26}$$

Appropriate shifting of rows and columns is all that is required to add the local element matrices directly into the global system matrix, $[B(\zeta)]$. Here, $\{G_0\}$, is a column vector of length $8(NZ)(NX)(NY)$, $[B(\zeta)]$ is the $8(NZ)(NX)(NY) \times 8NZNXNY$ block tridiagonal stiffness matrix for the region, and $\{\Phi\}$ is a column vector of length $8(NZ)(NX)(NY)$, containing the acoustic pressure field and it derivatives at the finite element nodes. Note that $[B(\zeta)]$ contains the yet undetermined impedance ζ, and $\{G_0\}$ contains the effects of the sound source, $G_0(x,y)$. Equation (26) is solved using PARDISO (a state-of-art, parallel, sparse solver, with equation reordering to minimize fill-in). The solution obtained from Eq. (26) is referred to as the FEM solution in the main body of this paper.